Radiation Physics and Chemistry 179 (2021) 109173

Contents lists available at ScienceDirect

Radiation Physics and Chemistry

journal homepage: www.elsevier.com/locate/radphyschem

The influence of radiation damage on electrons and ion scattering measurements from PVC films

B.P.E. Tee[a], M. Vos[b,*], H. Trombini[c], F.F. Selau[c], P.L. Grande[c], R. Thomaz[c,d]

[a] Department of Nuclear Physics, Research School of Physics, Australian National University, Canberra, Australia
[b] Electronic Materials Engineering, Research School of Physics, Australian National University, Canberra, Australia
[c] Ion Implantation Laboratory, Institute of Physics, Federal University of Rio Grande do Sul, Porto Alegre, RS, Brazil
[d] School of Technology, Pontifical Catholic University of Rio Grande do Sul, PUCRS, Porto Alegre–RS, Brazil

ARTICLE INFO

Keywords:
reflection electron energy loss spectroscopy
Polyvinyl chloride
Radiation damage

ABSTRACT

Polyvinyl chloride (PVC) is a material that decomposes rapidly when irradiated by charged particles. Here we use energy spectra of electrons reflected from the PVC films during electron radiation to monitor this process. This is accomplished by measuring the energy distribution of elastically scattered electrons which depends on the mass of the scattering atoms. Incoming electrons with energy between 5 and 40 keV are used. Information is obtained about both the relative amount of Cl, C and H present in the sample. Especially the Cl concentration decreases quickly during irradiation. At larger energy losses the signature of the band gap is visible in the energy loss spectrum. The number of excitations within the band gap increases rapidly when the composition of the film changes. The H intensity is somewhat less affected by the electron beam than the Cl intensity but accurate determination of the H content is complicated due to the changing background. Medium-energy ion scattering measurements (using 200 keV protons) and Rutherford backscattering measurements (using 2 MeV He ions) showed a strong decrease in the measured Cl intensity with ion fluence used. The Cl concentration as a function of fluence for electrons, protons and He ions can be described in a uniform way by considering the density of electronic excitations produced under the different irradiation conditions.

1. Introduction

Radiation damage in materials is an extensive field of research. Fast charged particles penetrating matter will interact with both the target nuclei and electrons. The energy transferred to the system may result in breaking of chemical bonds and volatile species may escape. Often these effects are detrimental, e.g. for studying organic samples in an electron microscope and sometimes they are utilised on purpose, e.g. in lithography (Tseng et al., 2003; Watt et al., 2007) and charged-particle based cancer treatment (Nikjoo et al., 2012).

Changes in sample composition with fluence have been studied using a wide array of experimental techniques. Using electron beams it can be observed as changes in the energy loss spectrum (Egerton et al., 1987; Reimer, 1984; Egerton, 2017, 2019) or changes in energy-dispersive x-ray analysis (EDX) (Vesely, 1984). The same is true for ion beam measurements where, for example, one has to be careful to obtain the correct composition of a polymer such as polyvinyl chloride (PVC) by Rutherford backscattering (Rickards et al., 1995), or proton induced x-ray emission (PIXE) measurements (Rickards and Zironi, 1991). Some samples change even under x-ray irradiation as can be observed by XPS (Takaoka et al., 2002).

Here we explore the possibilities of electron Rutherford backscattering (ERBS), in combination with reflection energy loss spectroscopy (REELS) to obtain a picture of both the elemental composition and electronic structure as a function of irradiation fluence, using PVC as an example. PVC is a widely used polymer and its interaction with radiation has been extensively studied (Wypich, 2020; Rangel et al., 2011). ERBS relies on the energy transfer in large-angle elastic scattering of keV electrons from nuclei (recoil effect) and can be used to observe H as well as C and Cl (Went and Vos, 2008). The same spectra also contain a signature of the electronic structure, e.g. it shows the band gap, i.e. the minimum energy loss observed in the spectra develops as a function of fluence (Vos et al., 2016).

One of the earliest application of ERBS was the determination of the H content in polyethylene and formvar (Chatzidimitriou-Dreismann et al., 2003; Vos et al., 2005). The H concentration was found to be less than the known stoichiometry but surprisingly agreed with the strength of the H signal as observed in deep inelastic neutron scattering,

* Corresponding author.
E-mail address: maarten.vos@anu.edu.au (M. Vos).

https://doi.org/10.1016/j.radphyschem.2020.109173
Received 5 July 2020; Received in revised form 30 August 2020; Accepted 1 September 2020
Available online 24 September 2020
0969-806X/

resulting in speculation that these deviations were a consequence of new quantum effects (attosecond quantum entanglement of protons) in the scattering process (Chatzidimitriou-Dreismann et al., 2003; Vos et al., 2005). No such deviations were found for gas-phase ERBS studies of CH_4, where the target is continuously replenished (Vos et al., 2008). Here the results of PVC will be used to revisit these earlier polymer ERBS results and investigate if it is possible to describe the deviations of the observed intensities from the expected one in terms of radiation damage.

2. Experimental procedure

A 130 nm-thick PVC layer was deposited on a Si wafer by spin coating from a solution of PVC (M_w = 80,000 u, supplied by Sigma Aldrich) in cyclohexanone for the electron beam experiment, while a 20 nm-thick PVC layer was deposited on silicon dioxide SiO_2 (100 nm thick film thermally grown on Si substrates) for the ion beam experiments.

The samples were measured using electron Rutherford backscattering in two different scattering geometries. Using a backscattering geometry (θ_{scat} = 135°) it was possible to separate the Cl and C signal of the elastic peak (i.e. that part of the spectrum that corresponds to scattered electrons that did not generate electronic excitations) for energies (E_0) between 20 and 40 keV due to the mass dependence of the recoil energies.

The H contribution can not be resolved under these conditions, as it contributes as a very weak, broad signal at very large energy loss values (≈ 38 eV (E_0 = 20 keV) to ≈ 78 eV (E_0 = 40 keV)) where it is superimposed to a much stronger signal due to elastic scattering from Cl or C plus additional electronic excitations. The H atoms can be detected by using a lower energy (5–15 keV) and a smaller scattering angle (θ_{scat} = 45°) as then the H contribution to the elastic peak (recoil loss from 1.6 to 4.8 eV) coincides to the band gap region for electrons scattered from C and Cl. Under these conditions it is not possible to separate the C and Cl contribution to the elastic peak (splitting for these elements is only 0.27 eV at 15 keV at this scattering angle).

In some cases a sub-monolayer of Au was evaporated on the PVC samples. At high energies and 135° scattering angle the Au contribution can be separated from the other elements present. This aided in determining the zero point of the energy scale accurately. With this knowledge it was possible to decompose the elastic peak in a contribution of Cl and Si from the substrate, as the contribution of the substrate became substantial after the majority of the Cl had been depleted from the sample.

After irradiation the beam spot area could be clearly identified under an optical microscope and it was found to have an area of 0.025 mm^2. Beam currents were between 5 and 10 nA for the 20–40 keV (θ_{scat} = 135°) measurement and between 10 and 100 pA for the 5–15 keV measurement at θ_{scat} = 45°.

The inelastic mean free path (IMFP) at 40 keV in PVC is expected to be close to 68 nm as derived from the (relativistic) TPP formula (Shinotsuka et al., 2016). For the incident beam along the surface normal the minimum length inside the PVC film for an electron scattering from the interface is then (1 + 1/cos45) × 130 = 314 nm i.e. 4.5 times the mean free path, which means that the signal from below the interface is attenuated by $e^{-4.5}$ i.e a factor of 90.

As we will see, after irradiation the film composition changes. If chlorine and/or hydrogen escapes the mass of the film will decrease. The final state after prolonged irradiation is most likely a carbon (graphite) film. Based on the initial number of carbon atoms present and the density of graphite this film would only be 28 nm thick. The IMFP of graphite at 40 keV is 37 nm (Shinotsuka et al., 2016). The effective path length for electrons scattered from the interface is then only 1.8 times the IMFP and the attenuation of the substrate signal is only a factor 6.

While we do not expect to fully carbonize our samples in these experiments, we can expect the substrate to contribute more to the elastic peak after prolonged radiation. For measurements at lower energies (e.g. 20 keV) and more glancing (more surface-sensitive) geometries the contribution of the Si substrate always remains low. The Si peak partly overlaps the Cl peak, but, as we will see, both contributions can be determined by curve fitting.

Ion scattering experiments were carried out using the Rutherford Backscattering Spectrometry (RBS) and Medium-Energy Ion Scattering (MEIS) techniques at the Ion Implantation Laboratory of the Federal University of Rio Grande do Sul (UFRGS). For the RBS a 2 MeV He^{2+} was used incident normal to the sample surface. The backscattering ions were detected by a solid-state detector (energy resolution of 15 keV) at 165°. The sample was kept inside the analysis chamber with a pressure of ≈ 10^{-7} mbar.

For the MEIS experiment a 500 kV electrostatic accelerator provided a H^+ beam with nominal energy of 200 keV incident along the surface normal. The detection system consisted of a Toroidal Electrostatic Analyzer (TEA) that collected the backscattered H^+ ions. At the exit plane of the TEA a set of two micro-channel plates coupled to a position-sensitive detector allowed the determination of the scattering energy and angle for each impinging ion (Smeenk et al., 1982; Tromp et al., 1984). This detection system was centered at 120° (angular aperture of 24°) with respect to the incident beam. The overall energy resolution of the system was 800 eV for 200 keV H^+. The samples were mounted on a three-axis goniometer, kept inside the analysis chamber under a pressure of about 10^{-8} mbar. For both the MEIS and RBS experiment the typical beam current was ~ 1 nA.

3. Electron beam results

Measurement of the elastic peak with a composition that approaches the nominal stoichiometry was only accomplished by adding spectra obtained from many different spots together. For the spectrum shown in Fig. 1 the sample was moved every 3 s to a new spot. Using 40 keV, 10 nA current this corresponds to a maximum exposure of 30 nC/spot (or 0.12 mC/cm^2). The peak at slightly more than 2 eV energy loss is due to electrons scattered from Cl, near 6.5 eV due to C. The elastic

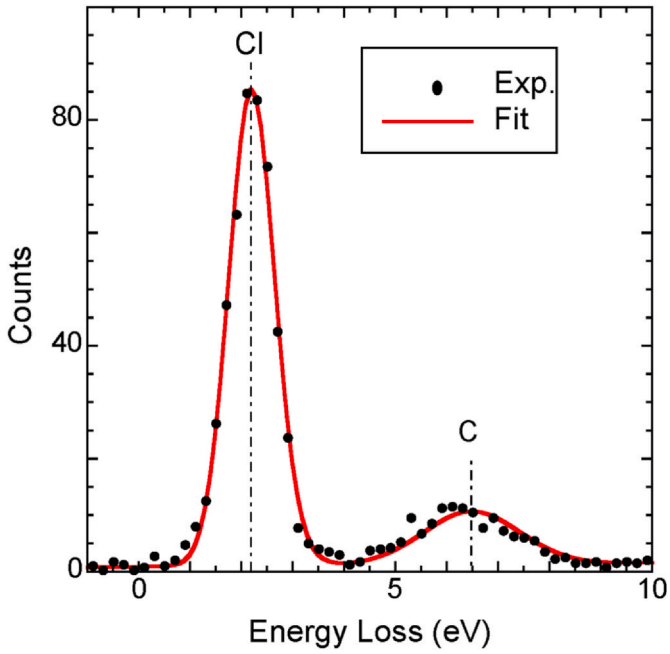

Fig. 1. The ERBS spectrum at 40 keV as obtained by taking the sum of spectra from multiple spots with for each spot a total fluence of 0.12 mC/cm^2. The intensity ratio of the carbon and Cl peak is within 5% of the expectation based on a composition of $(-C_2H_3Cl-)_n$.

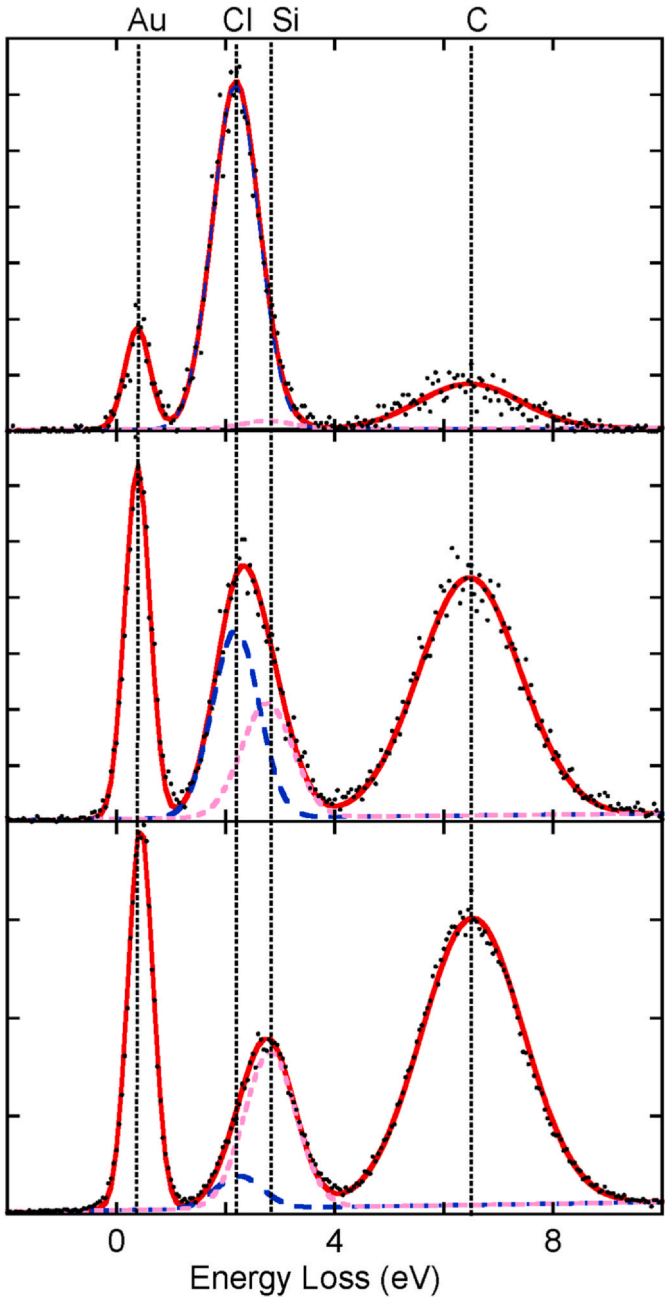

Fig. 2. The ERBS spectrum (dots) of a PVC film on which a 0.013 nm Au layer was evaporated. The spectra were taken at 40 keV and obtained after a fluence of 1.2 mC/cm^2 (top), 5.5 mC/cm^2 (central panel) and 135 mC/cm^2 (lower panel). The full line is based on a fit assuming the presence of Au, Cl, Si and C atoms. The Cl peak (long, blue dashed line) almost completely disappears after high fluence irradiation and the Si of the substrate becomes visible (purple, short dashed line). (For interpretation of the references to colour in this figure legend, the reader is referred to the Web version of this article.)

scattering cross section was obtained from a partial wave analysis (Salvat, 2003), and the Differential Cross Section (DCS) of Cl is ≈ 8times larger than the DCS of C (DCS values under these conditions are close to the Rutherford values i.e. are proportional to Z^2). Then for the stoichiometry ($C_2H_3Cl_y$) a value of $y = 0.98 \pm 0.05$ is obtained.

After longer exposure to the electron beam there are several changes to the spectrum. The peak near 2 eV energy loss (the 'Cl elastic peak') decreases strongly in intensity and there is a small shift of this peak to larger loss values. This small shift is especially evident for the sample on which a small amount of Au was evaporated (see Fig. 2) which helps to

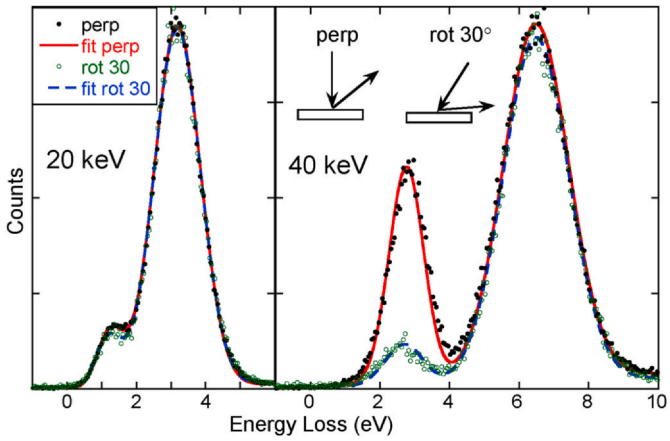

Fig. 3. The ERBS spectrum (dots) taken at 20 keV (left panel) and at 40 keV (right panel) after irradiation with 200 mC/cm^2 measured in a bulk-sensitive (perpendicular) and a surface sensitive (rotated 30°) geometry. At 40 keV in the bulk sensitive geometry the Si substrate is the main contributor to the high-energy elastic peak. The fact that at 20 keV the high-energy elastic peak hardly depends on the geometry means that it is due to the remaining Cl atoms.

determine the exact zero point of the energy scale. The interpretation of this is that with increasing amount of Cl depletion the attenuation of the Si elastic peak becomes less and Si starts contributing more to the peak near 2 eV energy loss. As the mean energy loss of electrons scattered from Si under these conditions is 0.6 eV larger than that of electrons scattered from Cl the increased visibility of Si causes the apparent shift of the combined elastic peak to larger loss values. Using peak fitting we can determine the Si and Cl peak area and from this the Cl to C peak area ratio and hence the Cl depletion. For a large fluence the Si contribution dominates the peak, but a small Cl contribution remains required for a good fit.

This interpretation is supported by rotating the sample to a more surface sensitive geometry (Fig. 3). Then the Si contribution to the peak at 2 eV energy loss is always severely attenuated, and only the Cl contribution remains. For the 20 keV measurement the mean free path is almost half that at 40 keV, and then the rotation causes only a very small difference, as at that beam energy the film remains thick enough to attenuate the Si signal strongly in both geometries.

The Cl peak intensity, as obtained after fitting the 2 eV loss feature with a Si and a Cl component, was monitored as a function of fluence x and the obtained curve is shown in Fig. 2. The measurement was done in 3 different geometries, probing an effective depth that changes by more than a factor of 2, but a very similar decay of the Cl signal was obtained in all three cases.

As is clear from Fig. 4 the Cl concentration did not follow a simple exponential decay. Indeed, several models for Cl depletion after charged particle irradiation are discussed in the literature, see e.g. (Vesely, 1984). In appendix A we show how several simple models lead to different functional forms for the Cl concentration. One such model suggests fitting with 2 fractions, each with a different exponential decay can describe the experimental observations:

$$\frac{N_{Cl}(x)}{N_{Cl}(0)} = (1 - A)e^{-k_1 x} + Ae^{-k_2 x}. \quad (1)$$

Our experimental findings can indeed also be described quite well (except at very high exposure) using two fractions with a different exponential decay, see the fit in Fig. 4.

A variation of this model is when one considers as trap sites those C atoms that have lost a Cl atom. This leads to an expression:

$$\frac{N_{Cl}(x)}{N_{Cl}(0)} = e^{-k_1 x}(1 - fk_1 x) + fN_0\left(1 - e^{-k_1 x}\right). \quad (2)$$

Note that this model has only two adjustable parameters as the

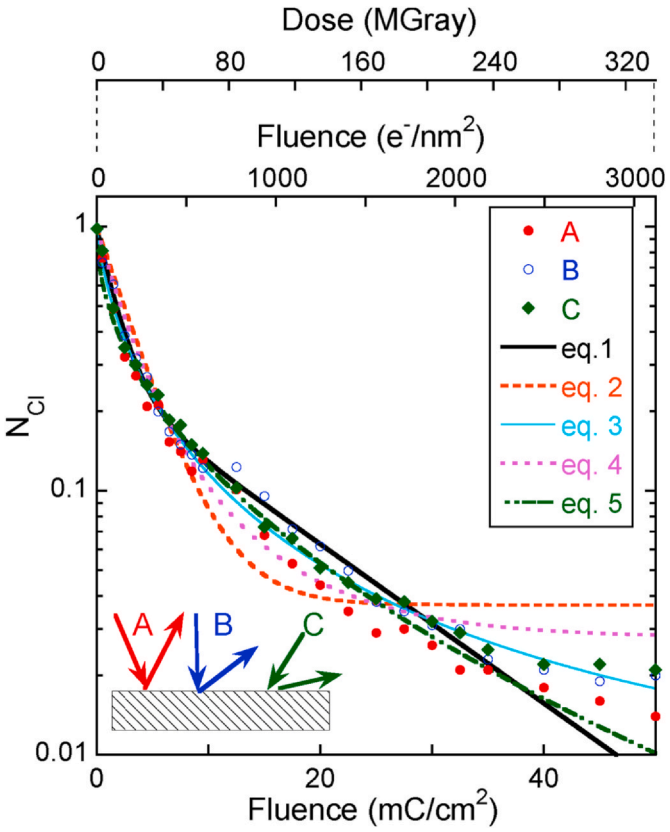

Fig. 4. The number of Cl atoms present for every 2 C atoms (N_{cl}) as a function of radiation fluence for 40 keV electrons in 3 different measurement geometries, as sketched, using a film with some gold evaporated on the surface. The dose-dependence is fitted with 5 models described in the main text (See Table 1, for values used). The dose in Gray is calculated using the density and stopping power of pristine PVC. (For interpretation of the references to colour in this figure legend, the reader is referred to the Web version of this article.)

k_2(detrapping) is obviously equal to k_1. This model does not describe the experimental observation very well.

In a model suggested by Veseley (Vesely, 1984) the decay rate is not constant but is assumed to reduce with fluence. If k_1 is the initial decay rate and k_2 describes the fluence dependence of the decay rate then one gets a Cl content proportional to:

$$\frac{N_{Cl}(x)}{N_{Cl}(0)} = e^{-k_1\left(e^{-k_2 x^n}\right)x}. \tag{3}$$

This approach gives a good description up to the highest fluence used here but only if n is varied from the value of 1.

A related formula, also based on the decrease in decay rate with fluence, is derived in appendix A. It reads:

$$\frac{N_{Cl}(x)}{N_{Cl}(0)} = e^{-k_1 f(x)x}, \tag{4}$$

with $f(x) = (1 - \exp(-k_2 x))/(k_2 x)$. As can be seen in Fig. 4 this approach describes the observed data quite well.

Finally, in the context of carbon loss in a electron microscope the following formula was suggested (Dubochet, 1975):

$$\frac{N_{Cl}(x)}{N_{Cl}(0)} = e^{-k_1 x/x^n}. \tag{5}$$

It gives the best description of the models with only 2 adjustable parameters.

We investigated if there were any differences in Cl depletion for a beam current of 1 nA and 10 nA. We found similar decrease in Cl intensity scaled with the accumulated charge and no clear influence of the actual beam current used was found.

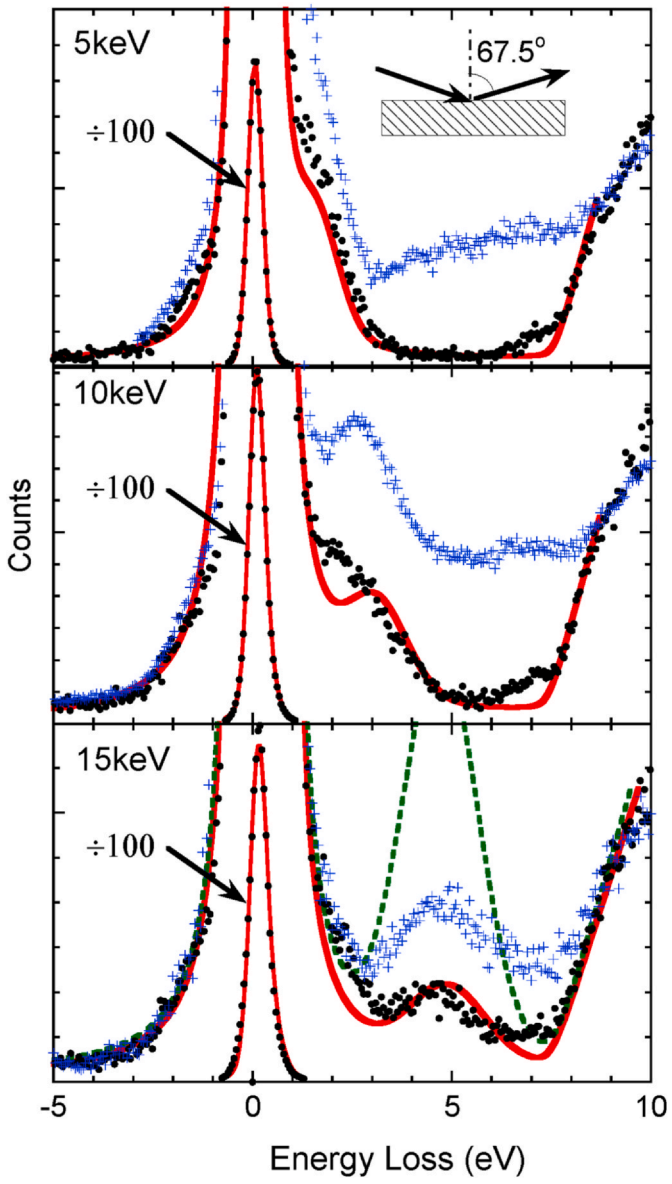

Fig. 5. The spectra obtained for a scattering angle of 45° at the incoming energies as indicated. After the main elastic peak the low intensity region extending up to 7.5 eV corresponds to the band gap. The small peak visible at an energy loss increasing proportional to the incoming beam energy corresponds to the elastic peak of H (dots). The red line is the calculated spectrum assuming the nominal atomic composition of PVC. The blue + signs are the spectrum after a fluence of 0.6 mC/cm^2 (5 keV), 0.8 mC/cm^2 (10 keV) and 0.7 mC/cm^2 (15 keV) and with the main elastic peak normalised to the same area. The H area looks more intense as the main peak is less strong due to the severe depletetion in Cl. Moreover, the intensity in the band gap area has increased strongly, indicating that the sample is not an insulator anymore. The dashed green line in the 15 keV panel is the expected spectrum for C_2H_3, i.e all Cl but no H removed. The measured H intensity after irradiation is far from this limit. (For interpretation of the references to colour in this figure legend, the reader is referred to the Web version of this article.)

In principle it is possible that the small amount of Cl visible after prolonged irradiation could be due to the halo (i.e. region of low electron density around the beam, present for most electron beams. It originates from the interaction between different electrons inside the beam, changing slightly their direction of propagation.) The halo interacts with a part of the film that has seen a much smaller fluence. To

test this we moved the sample by half the beam diameter up-down and left-right and irradiated a square area consisting of 9 spots in this way. Returning to the central spot there was still a similar amount of Cl visible after long exposure. Hence the tail in the Cl concentration in Fig. 4 can not be explained as a halo effect.

Using a geometry with a smaller scattering angle and lower energy beam it was possible to detect the elastic peak of hydrogen (Fig. 5). Due to the glancing in and glancing out geometry (angle of the incoming and outgoing beam with the surface normal is 67.5°) and lower incoming energy the contribution of the Si substrate should always be negligibly small, and changes in the mean free path of the irradiated PVC layer will affect the C, H and Cl intensity in the same way. As expected the H peak is very small, compared to the main elastic peak, due to the Cl and C contributions, not resolved under these conditions. Fully qualitative analysis is difficult, as the H peak either partially overlaps with the main elastic peak (at 5 and 10 keV) or overlaps with the onset of the energy loss part of the spectrum. This onset (corresponding to the band gap) is clearly visible at 7.5 eV below the main elastic peak. This value is in reasonable agreement with the 8.0 eV obtained by Tahir and Tougaard for PVC using lower energy REELS measurements (Tahir and Tougaard, 2012). The spectra were simulated assuming a linear increase of the inelastic part of the spectrum above the band gap as described elsewhere (Vos et al., 2015). The calculated spectrum (red line) resembles the measured result reasonably well considering the weakness of the H signal and some uncertainty in the exact shape of the tail of the main elastic peak.

At larger fluence the most striking change is the increase of intensity in the band gap region. Initially the intensity in the gap is indistinguishable from the intensity at the energy-gain site of the elastic peak, i.e. completely determined by the dark count rate of the detector. After a dose close to 0.5 mC/cm^2 the intensity inside the gap is of the same order as the height of the H elastic peak.

There is no sign that the intensity of the H elastic peak, expressed as a fraction of the main elastic peak decreases with time. On the contrary, there seems a modest increase in this intensity. This does not mean that the H contents of the film increases. As the Cl content of the film decreases, the main elastic peak becomes less strong, and this explains the apparent increase in strength of the H peak. As a reference we plot in the lower panel of Fig. 5 also the calculated elastic peak of $(C_2H_3)_n$ normalised again to the main elastic peak. Clearly the H intensity is much too high in this calculation, indicating that either not all Cl has escaped and/or some H has been removed.

4. Comparison of electron-beam induced Cl depletion with those observed in MEIS and RBS

Besides using electrons the chlorine content of PVC films can also be studied with more traditional ion scattering experiments such as MEIS and RBS. A problem with ion scattering experiments using PVC films on a substrate (a SiO_2 overlayer on Si wafer was used here) is that the weak C signal of the PVC film is superimposed on a much stronger Si signal. This makes it difficult to determine the ratio of the C and Cl intensity, and indeed if the intensity of Cl as seen at low fluence is representative for pristine PVC. Thus, rather than measuring the Cl to C intensity ratio as a function of fluence, one measures in ion beam experiments the changes in the number of Cl atoms present per unit area. A comparison of the ion beam and electron beam result can then be made if one assumes that the number of carbon atoms present in the film does not change.

The H and He ions used here have more energy than the electrons in ERBS, but in spite of this, due to their larger mass, the velocity of the ions is much less. As a consequence the ions have more time to interact with the target electron system and their stopping is larger. In Fig. 6 we show an estimate of the electronic stopping (the nuclear stopping is small under these conditions) for electrons, protons and alpha particles in PVC as provided by the NIST database (Berger et al., 2017). The

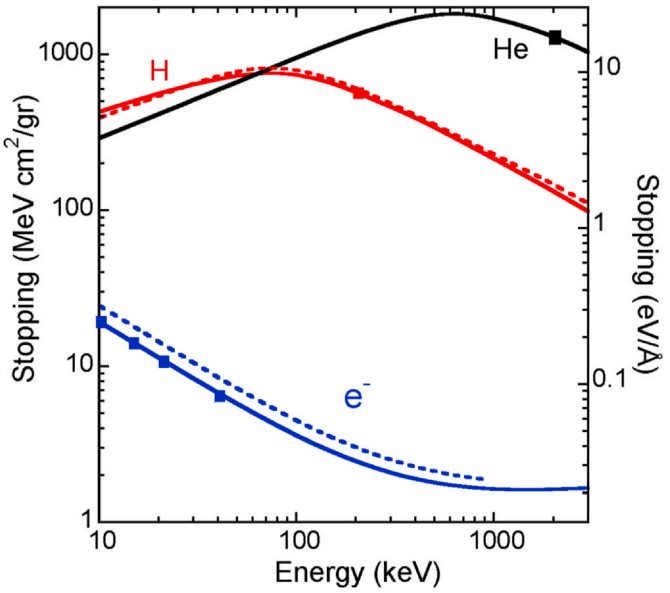

Fig. 6. The stopping for electrons and protons, as calculated using this fit to the ELF compared to that given in the PSTAR and ESTAR database and ASTAR data base from NIST. The dashed line is the calculated stopping for protons and electrons as discussed in appendix B. The boxes indicates energies used in the experiments described here.

200 keV protons used in the MEIS experiment have about 84 times larger stopping than 40 keV electrons, the 2 MeV He ions should have a stopping about 192 times larger than 40 keV electrons.

There are significant differences between the nature of the electronic excitations as induced by energetic electrons and ions, especially when the ions have energies near the stopping power maximum. This is discussed in appendix B. If one makes, in spite of this, the assumption that the release of chlorine is determined by the amount of energy deposited in the electronic excitations in the PVC film, then the same level of Cl depletion as in the electron case is then expected for a 84 times smaller proton fluence and a 192 times smaller He ion fluence.

This is illustrated in Fig. 7 where the measured Cl intensity is plotted with the same fit of Eq. (1) except that the fluence is scaled as the stopping power ratio. This works quite well for RBS but for MEIS the agreement is only reasonable if one allows for a constant offset which is attributed to the dark count rate of the channel plates used in the MEIS detector. This means that the Cl depletion is the same when the fluence is converted to joules deposited per kg material (Gray units), as is done in the top axis of Figs. 4 and 7.

5. Comparison to literature

The most widely quoted quantity is the initial decay rate of the Cl contents. Electron-beam induced depletion of chlorine was studied using the Cl LMM Auger (Auger energy 192 eV, the IMFP for this energy is approximately 10 Å) excited by a 10 keV electron beam by Lea et al. (2003). They observed a 10% decrease in Cl content near the surface after 0.07 mC/cm^2. As the IMFP is 3 times shorter at 10 keV, compared to 40 keV, one would expect for 40 keV electrons a 10% decrease at 0.21 mC/cm^2. We observe this reduction after a slightly larger dose of 0.3 mC/cm^2. Note that our experiment probes a layer that is 25 times thicker than the Auger experiment.

From the transmission experiment using 20 keV e$^-$ of Delgado and Hutchinson (1979) one gets a 10% decrease in intensity of the Cl Kα X-rays for a dose of 0.4 mC/cm^2. Correcting for the projectile mean free path this would be comparable to a dose of 0.7 mC/cm^2 in our experiment, thus their initial decay rate is slower than the one reported here.

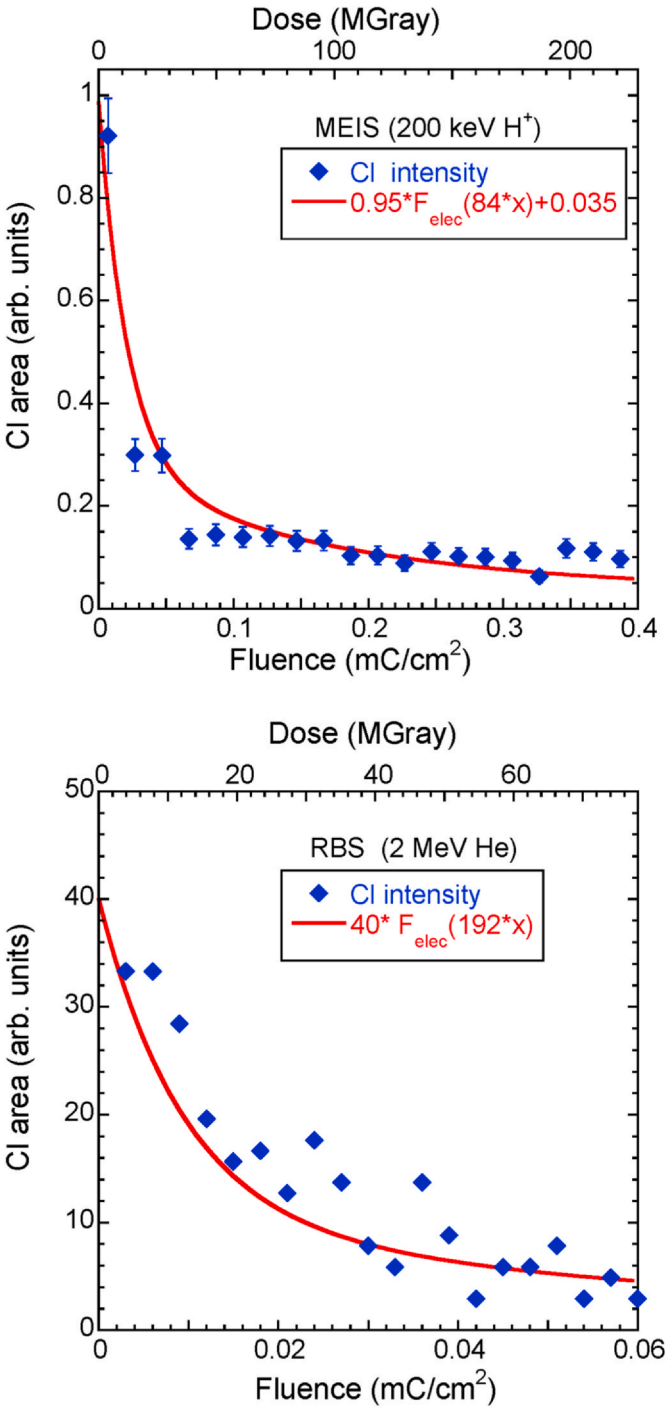

Fig. 7. The Cl intensity as measured by MEIS (top) and RBS (bottom) together with the decay curve as determined by ERBS (using Eq. (1)) but scaled for the horizontal axis according to the ratio of electronic stopping of e^- and the ion used. For MEIS a small quantity (0.035) was added corresponding to the dark count rate of the detector.

Lindberg et al. (1985) used a 200 keV electron beam to measure the decrease of the Cl X-ray intensity with dose. From their data one get a 10% decrease in Cl concentration for 0.8 mC/cm^2. This would correspond to a dose at 40 keV of 0.26 mC/cm^2 in good agreement with our results.

The measurement described here differ from those done in a transmission electron microscope due to the presence of a substrate. Firstly, the substrate is a source of secondary electrons that can propagate into the PVC film and causes additional chlorine loss. This will enhance the Cl loss as a function of fluence. However, the presence of two surfaces in a transmission experiment, will make it easier for the chlorine to escape into the vacuum and this could decrease the amount of Cl that gets re-trapped in the film.

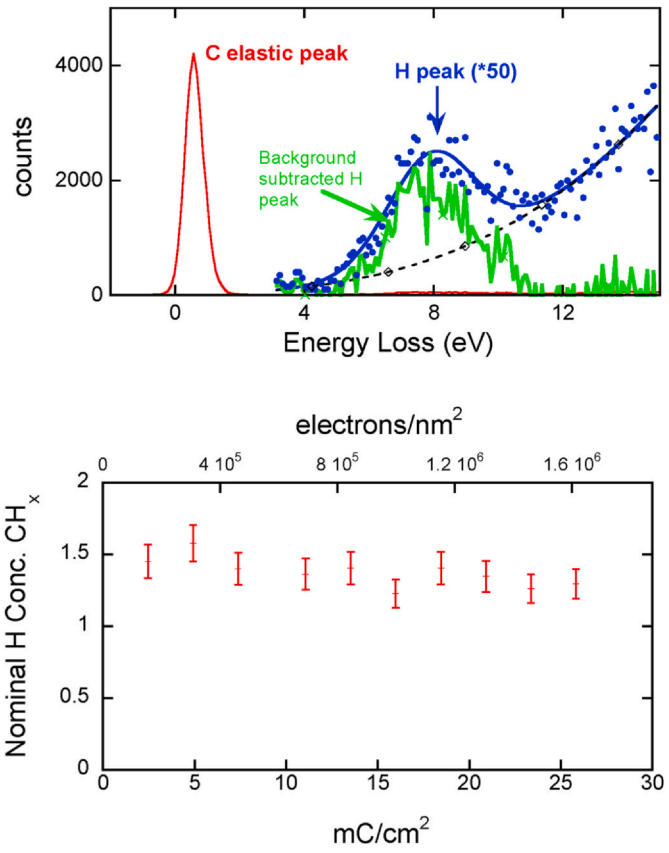

Fig. 8. The spectrum (top) of 25 keV electrons scattered over 45° as published in ref (Vos et al., 2005) and the derived H content in polyethylene $(-CH_{-2})_n$ as a function of fluence. The H content decreases slowly with increasing fluence but even for the lowest fluence the H content was significantly below the nominal stoichiometry.

From the literature ion irradiation measurements of PVC we mention in particular the work of Rickards et al. (1995), which provides information about the Cl/C ratio and the H/C ratio. They showed that the Cl contents decreased by a factor of 3–4 after a fluence of 1 mC/cm^2 using 3 MeV H^+. As the electron stopping at 40 keV e^- is 14 times smaller than 3 MeV protons (see Fig. 6) the corresponding electron beam dose would be 14 mC/cm^2. For this dose which we find a decrease by a factor of 10 (see Fig. 4), substantially larger. For the H to C ratio was Rickards et al. found a 20% decrease for the H/C ratio for a fluence of 1 mC/cm^2. The much slower decrease of H in comparison to Cl is in agreement with our measurements.

6. Comparison to polyethylene

For convenience we reproduce in Fig. 8 (top) a spectrum of polyethylene (PE) and the measurement of its H contents as a function of fluence (Vos et al., 2005). Clearly (see Fig. 8 (bottom)) the H concentration was always lower than expected. The lowest dose used for the measurement of the Cl concentration in PVC is much lower than for the measurement of the H concentration in PE. One interpretation of this figure is that the decay of H is also described by two exponential decay processes but the fast decay process is very quick (quicker even that the Cl decay) and hence was completed well before the first measurement was finished, and that thus a measurement of undamaged PE did not occur. The Cl measurement in PVC is comparatively easy, as

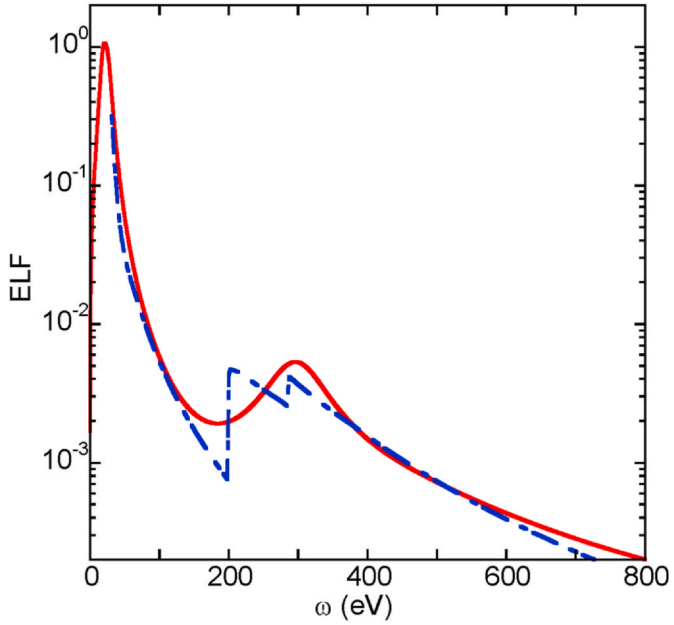

Fig. 9. The loss function in the optical limit used to calculate the electron and proton stopping. At low losses the Loss function coincides with the one given bydielectric function of Tahir and Tougaard (Tahir and Tougaard, 2012), and follows at higher losses the one derived from Henke (Henke et al., 1993).

Table 1
Fitting parameters used for the fits shown in Fig. 4.

	k_1	k_2	A,n,f
	Cm^2/n	Cm^2/nC	
Eq. (1)	0.56	0.072	A = 0.24
Eq. (2)	0.029	–	f = 0.037
Eq. (3)	2.0	1.3	n = 0.23
Eq. (4)	0.36	0.10	–
Eq. (5)	0.68	–	n = 0.51

Table 2
Parameters of the dielectric function used. The first two oscillators correspond to the ELF as given by Tahir (Tahir and Tougaard, 2012). The other oscillators were added to follow roughly the ELF as calculated using the database of Henke (Henke et al., 1993).

A_i	ω_i	Γ_i
0.343	20	11
0.347	25.8	14.3
1.4e-3	300	95
8e-4	400	500
3e-5	1100	1100

its elastic scattering cross section is much larger than H. We plan to investigate this further in the future.

7. Conclusion

We described a new method of assessing the change in sample composition as a function of radiation fluence. X-ray yield based methods can measure the change in intensity of a component very well, but it is harder to assess if the (initially) measured intensity corresponds indeed to the nominal stoichiometry. The present method compares the elastic peak intensities of C, Cl and H, with energies that differ by only a few eV, i.e. the assumption that the IMFP of the signal and their detection efficiency are the same is very good. The cross sections, based on partial wave calculations are well established. Thus it is a critical test to see if the initial sample composition can be measured successfully. With some effort (taking the sum of many very short exposure measurements at different spots) this was indeed accomplished. Measurements in different geometries (and thus probing different depth) showed similar Cl depletion profiles. Moreover a good agreement was found with Cl depletion based on Cl LMM Auger electrons (energy ≈ 190 eV), a method which is an order of magnitude more surface sensitive.

Ion beam based measurements should also be able to determine the absolute stoichiometry. However, the transmission measurement of ref. (Rickards et al., 1995) using protons at a high energy where their scattering cross section deviated strongly from Rutherford, and an absolute determination of the stoichiometry at low fluence was not made. Ion beam measurements using thin films on substrate have to recover the C intensity which generally will be superimposed on the stronger substrate signal. In the electron beam experiment the substrate only

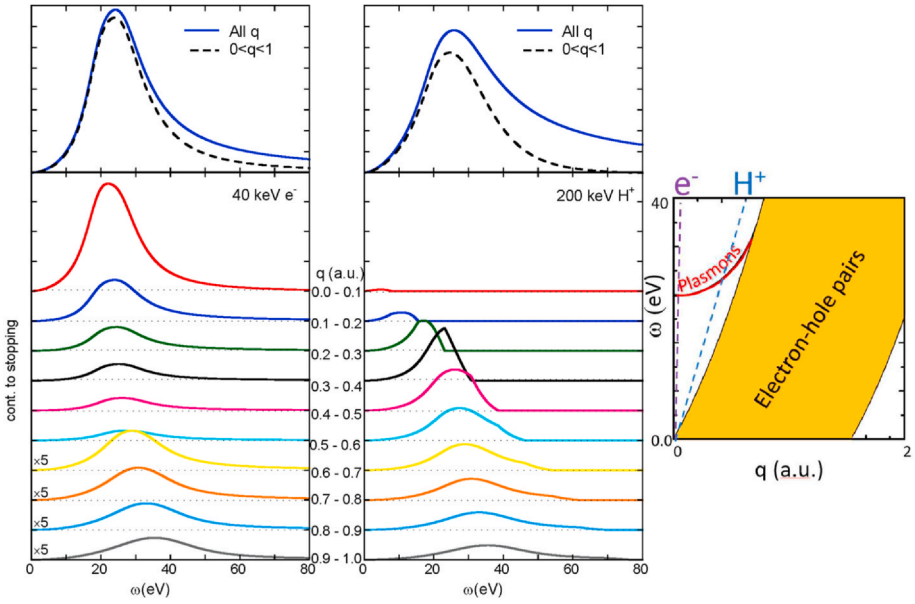

Fig. 10. The contribution to the stopping (i.e. proportional to $\omega \mathrm{Im}[-1/\varepsilon(\omega, q)]$) integrated over a range of q values, as indicated for both 40 keV e^- (left panel) and 200 keV H^+ (central panel) in PVC. Although both described by Eq. (16) their distribution over momentum is rather different. The right panel shows a simplified picture how the plasmons (red line) and electron-hole excitations (yellow shaded area) contribute to the loss function. Only the loss function to the right of the dashed line (from Eq. (17), marked e^- and H^+) contribute to stopping. (For interpretation of the references to colour in this figure legend, the reader is referred to the Web version of this article.)

plays a role at high energies in a bulk-sensitive geometry, and even then the substrate contribution can be established by curve fitting.

The H intensity was monitored as well. Its increase in intensity (relative to the main elastic peak due to C and Cl) was attributed to the escape of Cl. The intensity within the band gap, due to inelastic excitations, seen at the same energy as the H elastic peak, showed a strong increase with fluence. Desorption of the Cl is thus accompanied by a decrease of the insulating properties of the film.

Electron scattering at high energies can thus provide insight in several aspects of radiation damage and the results can be interpreted consistently with those obtained from ion-scattering experiments. The scaling of Cl depletion with electronic stopping could well be only approximate as, when calculated within the dielectric formalism (see appendix B), the excitation distribution over energy loss and momentum is rather different, especially for low-energy ions. A more detailed test here would be relevant e.g. for medical physics microdosimetry.

CRediT authorship contribution statement

B.P.E. Tee: did the measurement with the electron beam. **M. Vos:** Supervision, Writing - original draft. **H. Trombini:** was responsible for the MEIS measurements. **F.F. Selau:** did the RBS measurements. **R. Thomaz:** made the PVC film.

Declaration of competing interest

The authors declare that they have no known competing financial interests or personal relationships that could have appeared to influence the work reported in this paper.

Acknowledgments

This study was financed in part by the Coordenação de Aperfeiçoamento de Pessoal de Nível Superior - Brasil (CAPES) - Finance Code 001, by Conselho Nacional de Desenvolvimento Científico e Tecnológico (CNPq) and PRONEX-FAPERGS. MV acknowledges the ARC funding program for financial support.

Appendix A. Some simple models

The simplest model is that all Cl atoms escape after the C–Cl bond is broken due to the irradiation. The number of C–Cl bonds that is broken under irradiation is then proportional to N_{cl}, the number of Cl atoms present:

$$\frac{dN_{Cl}}{dx} = -k_1 N_{Cl}. \tag{6}$$

This predict an exponential decay.

One can further assume that not all Cl atoms escape immediately from the film after the C–Cl bond is broken but can be trapped at certain sites present in the film with concentration N_{tr}. The radiation can then subsequently cause the trapped atoms to detrap: The number of Cl atom trapped somewhere is given by:

$$\frac{dN_{Cl}^{tr}}{dx} = f k_1 N_{Cl} - k_2 N_{Cl}^{tr}, \tag{7}$$

where f is the trapped fraction and k_2 is detrapping rate. The solution of Eq. (6) and Eq. (7) for $N_{Cl} + N_{Cl}^{tr}$ is:

$$N_{Cl} + N_{Cl}^{tr} = (N_0 - a)e^{-k_1 x} + ae^{-k_2 x}, \tag{8}$$

with:

$$a = \frac{fk_1}{k_1 - k_2}. \tag{9}$$

This is a sum of two exponential functions i.e. this model leads to Eq. (1).

As a variation to this model one can assume that the trapping sites are those C atoms from which a Cl atom has been removed previously and after trapping the C–Cl bond is restored. Before the irradiation the trapping density is thus zero. The rate for trapping at sites formed by the C atoms with a chlorine missing is given by

$$\frac{dN_{Cl}^{tr}}{dx} = fk_1(N_0 - N_{Cl}) - k_1 N_{Cl}^{tr}, \tag{10}$$

where f is trapping fraction in this available sites and k_1 is detrapping rate, the same from C–Cl bonds. As long as $f < 1$ there is net reduction in Cl content.

The solution for $N_{Cl} + N_{Cl}^{tr}$ becomes then

$$N_{Cl} + N_{Cl}^{tr} = N_0 e^{-k_1 x}(1 - fk_1 x) + fN_0\left(1 - e^{-k_1 x}\right). \tag{11}$$

Finally one could consider that it becomes harder to remove Cl from the polymer if other Cl atoms along the chain are already missing. Eq. (6), describing a fluence dependent rate $k(x)$ of C–Cl bond breaking becomes then:

$$\frac{dN_{Cl}}{dx} = -k(x)N_{Cl}. \tag{12}$$

The solution of this equation is simply given by

$$N_{Cl}(x) = N_{Cl}(0)e^{-\int_0^x k(x')dx'}. \tag{13}$$

One could further assume that the change of $k(x)$ with fluence x is at a constant rate (k_2) according to:

$$\frac{dk(x)}{dx} = -k_2 k(x) \tag{14}$$

whose solution is just an exponential function

$$k(x) = k_1 \exp(-k_2 x). \tag{15}$$

Substituting Eq. (15) into Eq. (13) leads to Eq. (4).

Appendix B. Difference and similarities between electron and proton interaction with PVC

Here we want to explore how closely related PVC degradation by electron irradiation (as in the 40 keV ERBS experiment described here) and proton irradiation (at 100 keV and above, as is used in MEIS and RBS) are. In both cases the energy deposited in the target is dominated by interactions with the target electrons (electronic stopping) and can be described within the dielectric formalism. Within this formalism the interaction is described by a set of collisions separated (on average) by the inelastic mean free path.

Within the dielectric theory the stopping is given by:

$$\frac{dE}{dx} = \int_0^{E_{\max}} \omega W_b(\omega, E_0)d\omega = \int_0^{E_{\max}} \frac{2\omega\, d\omega}{\pi m v^2} \int_{q_{\min}}^{q_{\max}} \frac{dq}{q} \operatorname{Im}\left[\frac{-1}{\varepsilon(\omega, q)}\right], \tag{16}$$

with m the mass of a target electron and v the projectile velocity. The limits of integration are determined by energy and momentum conservation laws for the collision of the projectile (mass M) and the target electrons. For electrons $E_{\max} = E_0$ and

$$q_{\min} = \sqrt{2ME_0} - \sqrt{2M(E_0 - \omega)}, \tag{17}$$

corresponding to the momentum transfer due to the reduced energy, while there is no change in the projectile propagation direction. For protons $q_{\min}$ for a given energy loss is close to $\sqrt{M_p/M_e} \approx 42$ larger than for electrons with the same energy.

For energetic electrons relativistic corrections to $q_{\min}$ has to be incorporated as described by e.g. Shinotsuka *et al.* (Shinotsuka et al., 2015). For the upper limit it is customary to take for electrons

$$q_{\max} = \sqrt{2ME_0} + \sqrt{2M(E_0 - \omega)}, \tag{18}$$

corresponding to backscattering of the electron, whereas for protons the maximum q value is where one electron absorbs E_0 energy ($q_{\max} = \sqrt{2M_e E_0}$).

In order to calculate any of these value one needs a model for the loss function. Tahir and Tougaard published an estimate of the loss function in the optical limit ($\operatorname{Im}[-1/\varepsilon(\omega, q = 0)]$) for the low loss region of PVC using two Drude-Lindhard type oscillators (Tahir and Tougaard, 2012).

$$\operatorname{Im}\left[\frac{-1}{\varepsilon(\omega, 0)}\right] = \sum_i A_i \frac{\omega\Gamma_i\omega_i^2}{(\omega^2 - \omega_i^2)^2 + \omega^2\Gamma_i^2}. \tag{19}$$

As deeper levels contribute to stopping we extended their model with three more oscillators at larger energy loss, to approximately model the optical data of Henke (Henke et al., 1993), see Fig. 9. Describing deeper levels with a Generalized Oscillator strength could give slightly better results (Heredia-Avalos et al., 2005), but for simplicity the whole ELF is described here using a sum of similar oscillators. The parameters are given in

Table 2. Having fitted the ELF we have to decide how $\mathrm{Im}[-1/\varepsilon(\omega, q)]$ changes with q. For this it is best to re-interpret the Drude-Lindhard oscillators as Mermin oscillators (both coincide at $q = 0$) and use the q−dependence that is fixed ('build-in') for the Mermin model. This means we incorporate the electron-hole pairs branch of the dielectric function in the calculation and consider not just the plasmon. This improves the stopping calculation at low projectile energies (Abril et al., 1998). The results for electron and proton stopping are given as a dashed line in Fig. 6 and compare reasonably well with the Bethe theory results from the ESTAR, PSTAR database.

Assuming that the sample changes in PVC are from electronic stopping, then the naive expectation would be that the rate of change in sample composition (per nC/cm^2) in a proton and an electron beam experiment should relate as their stopping values. In reality it could be more complicated as the nature of the excitation created is different for both projectiles. To illustrate this we calculated the contribution to Eq. (16) for different q (momentum transfer) slices for a typical ERBS (40 keV e^-) and MEIS (200 keV H^+) case, see Fig. 10. Clearly in the electron case low-q excitations (plasmons) contribute much more to the stopping compared to the proton case. The probability that an excitation leads to the breaking of a Cl–C bond may well depend on the q value of the excitation. MEIS measurements are possible, in principle, for values somewhat below and above the stopping power maximum. Plasmon-type excitations become more prevalent for ion energies above the stopping power maximum (80 keV, see Fig. 6), whereas electron-hole type excitations, generally at larger q values, dominate at lower ion energies. Studying if the rate of Cl loss just scales as the electronic stopping may establish if the q−value of the excitation affects the Cl loss. If that is the case Cl depletion will be different for irradiation with protons at low and high energies for the same dose in Gray units.

References

Abril, I., Garcia-Molina, R., Denton, C., Pérez-Pérez, F., Arista, N., 1998. Dielectric description of wakes and stopping powers in solids. Phys. Rev. 58, 357. https://doi.org/10.1103/physreva.58.357.

Berger, M.J., Coursey, J.S., Zucker, M.A., Chang, J., 2017. Stopping-power and range Tables for Electrons, Protons, and Helium Ions. NIST Standard Reference Database 0.18434/T4NC7P.

Chatzidimitriou-Dreismann, C.A., Vos, M., Kleiner, C., Abdul-Redah, T., 2003. Comparison of electron and neutron Compton scattering from entangled protons in a solid polymer. Phys. Rev. Lett. 91https://doi.org/10.1103/PhysRevLett.91.057403. 57403.

Delgado, L.A., Hutchinson, T.E., 1979. Elemental loss during electron beam irradiation. Ultramicroscopy 4, 163. https://doi.org/10.1016/s0304-3991(79)90139-6.

Dubochet, J., 1975. Carbon loss during irradiation of T4 bacteriophages and E. coli bacteria in electron microscopes. J. Ultra. Res. 52, 276. https://doi.org/10.1016/s0022-5320(75)80118-3.

Egerton, R., 2017. Scattering delocalization and radiation damage in STEM-EELS. Ultramicroscopy 180, 115. https://doi.org/10.1016/j.ultramic.2017.02.007.

Egerton, R., 2019. Radiation damage to organic and inorganic specimens in the TEM. Micron 119, 72. https://doi.org/10.1016/j.micron.2019.01.005.

Egerton, R., Crozier, P., Rice, P., 1987. Electron energy-loss spectroscopy and chemical change. Ultramicroscopy 23, 305. https://doi.org/10.1016/0304-3991(87)90240-3.

Henke, B., Gullikson, E., Davis, J., 1993. X-ray interactions: photoabsorption, scattering, transmission, and reflection at E = 50-30,000 eV, Z = 1-92. Atomic Data Nucl. Data Tables 54, 181. https://doi.org/10.1006/adnd.1993.1013.

Heredia-Avalos, S., Garcia-Molina, R., Fernández-Varea, J.M., Abril, I., 2005. Calculated energy loss of swift He, Li, B, and N ions in SiO^2, Al^22O^3, and ZrO^2. Phys. Rev. 72https://doi.org/10.1103/physreva.72.052902. 052902.

Lea, S., Engelhard, M., Baer, D., 2003. Electron beam damage in poly(vinyl chloride) and poly(acrylonitrile) as observed by auger electron spectroscopy. Surf. Sci. Spectra 10, 67. https://doi.org/10.1116/11.20030904.

Lindberg, K.A.H., Vesely, D., Bertilsson, H.E., 1985. Chlorine loss and mass loss from polyvinylchloride and polyvinylidenchloride under the electron beam. J. Mater. Sci. 20, 2225–2232. https://doi.org/10.1007/bf01112308.

Nikjoo, H., Uehara, S., Emfietzoglou, D., 2012. Interaction of radiation with Matter. CRC press.

Rangel, E.C., dos Santos, N.M., Bortoleto, J.R.R., Durrant, S.F., Schreiner, W.H., Honda, R.Y., de Cássia, R., Rangel, C., Cruz, N.C., 2011. Treatment of PVC using an alternative low energy ion bombardment procedure. Appl. Surf. Sci. 258 (5), 1854–1861. https://doi.org/10.1016/j.apsusc.2011.10.061.

Reimer, L., 1984. Methods of detection of radiation damage in electron microscopy. Ultramicroscopy 14, 291. https://doi.org/10.1016/0304-3991(84)90097-4.

Rickards, J., Zironi, E., 1991. Chlorine loss from polyvinyl chloride under proton bombardment. Nucl. Instrum. Methods Phys. Res. Sect. B Beam Interact. Mater. Atoms 56, 687. https://doi.org/10.1016/0168-583x(91)95004-w.

Rickards, J., Trejo-Luna, R., Andrade, E., 1995. PVC film behavior under proton bombardment. Radiat. Phys. Chem. 45, 629. https://doi.org/10.1016/0969-806x(94)00080-4.

Salvat, F., 2003. Optical-model potential for electron and positron elastic scatteing by atoms. Phys. Rev. 68https://doi.org/10.1103/PhysRevA.68.012708. 012708.

Shinotsuka, H., Tanuma, S., Powell, C.J., Penn, D.R., 2015. Calculations of electron inelastic mean free paths. X. Data for 41 elemental solids over the 50 eV to 200 keV range with the relativistic full Penn algorithm. Surf. Interface Anal. 47, 871. https://doi.org/10.1002/sia.5789.

Shinotsuka, H., Da, B., Tanuma, S., Yoshikawa, H., Powell, C.J., Penn, D.R., 2016. Calculations of electron inelastic mean free paths. XI. data for liquid water for energies from 50 eV to 30 keV. Surf. Interface Anal. 49, 238. https://doi.org/10.1002/sia.6123.

Smeenk, R.G., Tromp, R.M., Kersten, H.H., Boerboom, A.J.H., Saris, F.W., 1982. Angle resolved detection of charged particles with a novel type toroidal electrostatic analyser. Nucl. Instrum. Methods Phys. Res. 195, 581. https://doi.org/10.1016/0029-554X(82)90022-2.

Tahir, D., Tougaard, S., 2012. Electronic and optical properties of selected polymers studied by reflection electron energy loss spectroscopy. J. Appl. Phys. 111https://doi.org/10.1063/1.3688327. 054101.

Takaoka, K., Koizumi, S., Maeda, S., Bureau, C., Endo, K., Hyodo, K., Miura, H., 2002. Surface damage of PVC polymers during XPS analysis. J. Surf. Anal. 9, 471. https://doi.org/10.1384/jsa.9.471.

Tromp, R.M., Kersten, H.H., Granneman, E., Saris, F.W., Koudijs, R., Kilsdonk, W.J., 1984. A new uhv system for channeling/blocking analysis of solid surfaces and interfaces. Nucl. Instrum. Methods Phys. Res. Sect. B Beam Interact. Mater. Atoms 4, 155. https://doi.org/10.1016/0168-583X(84)90055-7.

Tseng, A., Chen, K., Chen, C., Ma, K., 2003. Electron beam lithography in nanoscale fabrication: recent development. IEEE Trans. Electron. Packag. Manuf. 26, 141. https://doi.org/10.1109/tepm.2003.817714.

Vesely, D., 1984. Electron beam damage of amorphous synthetic polymers. Ultramicroscopy 14, 279. https://doi.org/10.1016/0304-3991(84)90096-2.

Vos, M., Chatzidimitriou-Dreismann, C.A., Abdul-Redah, T., Mayers, J., 2005. Electron and neutron scattering from polymer films at high momentum transfer. Nucl. Instrum. Methods B 227, 233–250. https://doi.org/10.1016/j.nimb.2004.09.003.

Vos, M., Went, M., Cooper, G., Chatzidimitriou-Dreismann, C., 2008. Elastic electron scattering from methane at high momentum transfer. J. Phys. B Atom. Mol. Opt. Phys. 41https://doi.org/10.1088/0953-4075/41/13/135204. 135204.

Vos, M., Marmitt, G., Finkelstein, Y., Moreh, R., 2015. Determining the band gap and mean kinetic energy of atoms from reflection electron energy loss spectra. J. Chem. Phys. 143https://doi.org/10.1063/1.4929911. 104203.

Vos, M., King, S.W., French, B.L., 2016. Measurement of the band gap by reflection electron energy loss spectroscopy. J. Electron. Spectrosc. Relat. Phenom. 212, 74–78. https://doi.org/10.1016/j.elspec.2016.08.001.

Watt, F., Breese, M.B.H., Bettiol, A.A., van Kan, J.A., 2007. Proton beam writing. Mater. Today 10, 20. https://doi.org/10.1016/s1369-7021(07)70129-3.

Went, M., Vos, M., 2008. Rutherford backscattering using electrons as projectiles: underlying principles and possible applications. Nucl. Instrum. Methods Phys. Res., Sect. B 266, 998–1011. https://doi.org/10.1016/j.nimb.2008.01.059.

Wypich, G., 2020. PVC Degradation and Stabilization, fourth ed. Chemtec Publishinghttps://doi.org/10.1016/C2014-0-01988-0.